Science Advances
AAAS

Supplementary Materials for

High-resolution structure and dynamics of mitochondrial complex I—Insights into the proton pumping mechanism

Kristian Parey, Jonathan Lasham, Deryck J. Mills, Amina Djurabekova, Outi Haapanen, Etienne Galemou Yoga, Hao Xie, Werner Kühlbrandt, Vivek Sharma*, Janet Vonck*, Volker Zickermann*

*Corresponding author. Email: vivek.sharma@helsinki.fi (V.S.); janet.vonck@biophys.mpg.de (J.V.); zickermann@med.uni-frankfurt.de (V.Z.)

Published 12 November 2021, *Sci. Adv.* **7**, eabj3221 (2021)
DOI: 10.1126/sciadv.abj3221

The PDF file includes:

Other Supplementary Material for this manuscript includes the following:

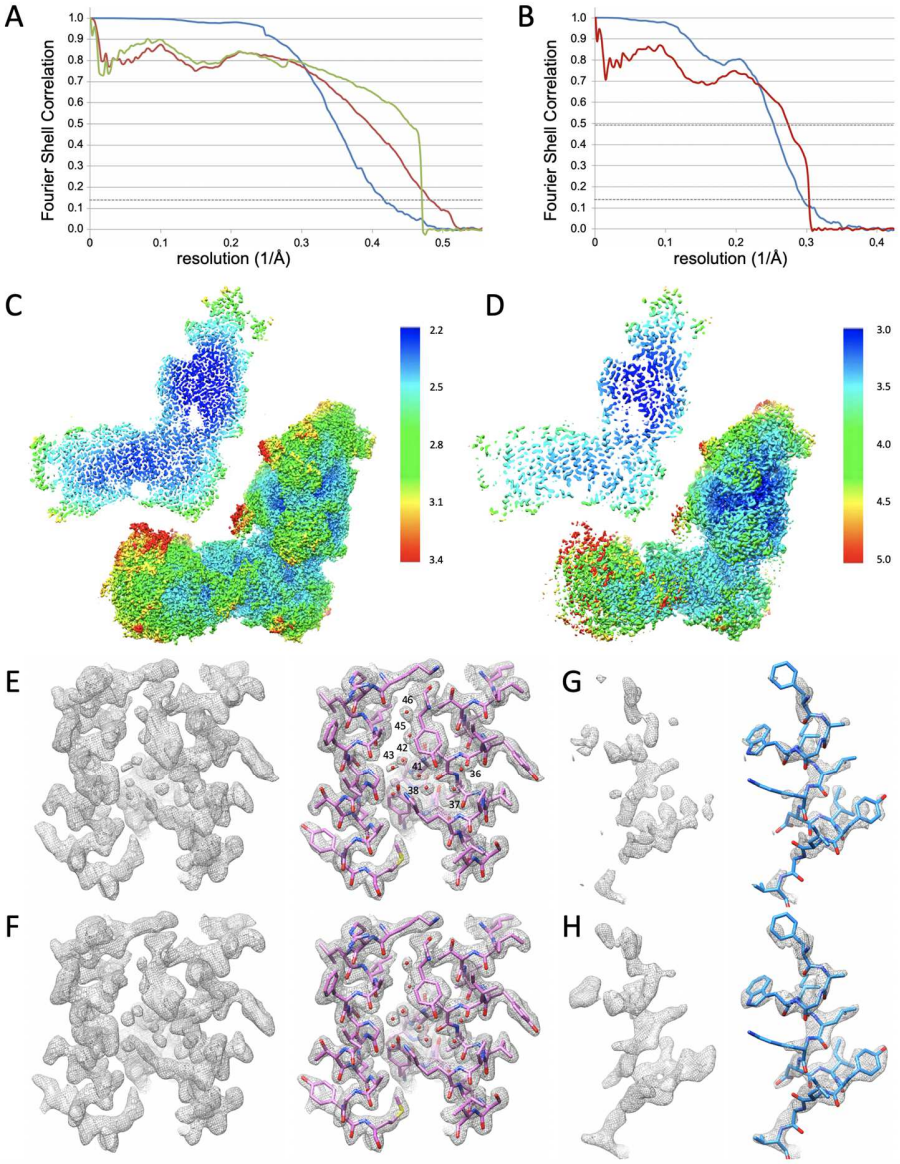

Figure S1. Map validation. (**A**) FSC plots for resolution estimation and model validation of wild type complex I. Gold-standard FSC plot between two half-maps separately refined in Relion (blue) indicates a resolution of 2.4 Å (0.143 threshold). Map-to-model FSC for the final refined model and the Relion map (red) and the density modified map (green) indicate a resolution of 2.5 and 2.2 Å, respectively (0.5 FSC criterion). (**B**) FSC plots for complex I under turnover. Gold-standard FSC (blue curve): 3.4 Å, map-to-model FSC (red): 3.6 Å. (**C**) Unmodified wt and (**D**) turnover cryo-EM map colored by local resolution as determined in Relion. Color scale in Å. (**E-H**) Details of the wt cryo-EM density before (**E,G**) and after (**F,H**) density modification in Phenix (Terwilliger 2020). Red spheres: water molecules. The procedure improved the average resolution of the map from 2.4 to 2.1 Å. It had subtle effects in high-resolution areas, especially making water densities stronger and more symmetric (detail of ND2, **E-F**, waters numbered as in figure S2F), while improving the continuity of less well resolved features (surface helix in ND5, **G-H**).

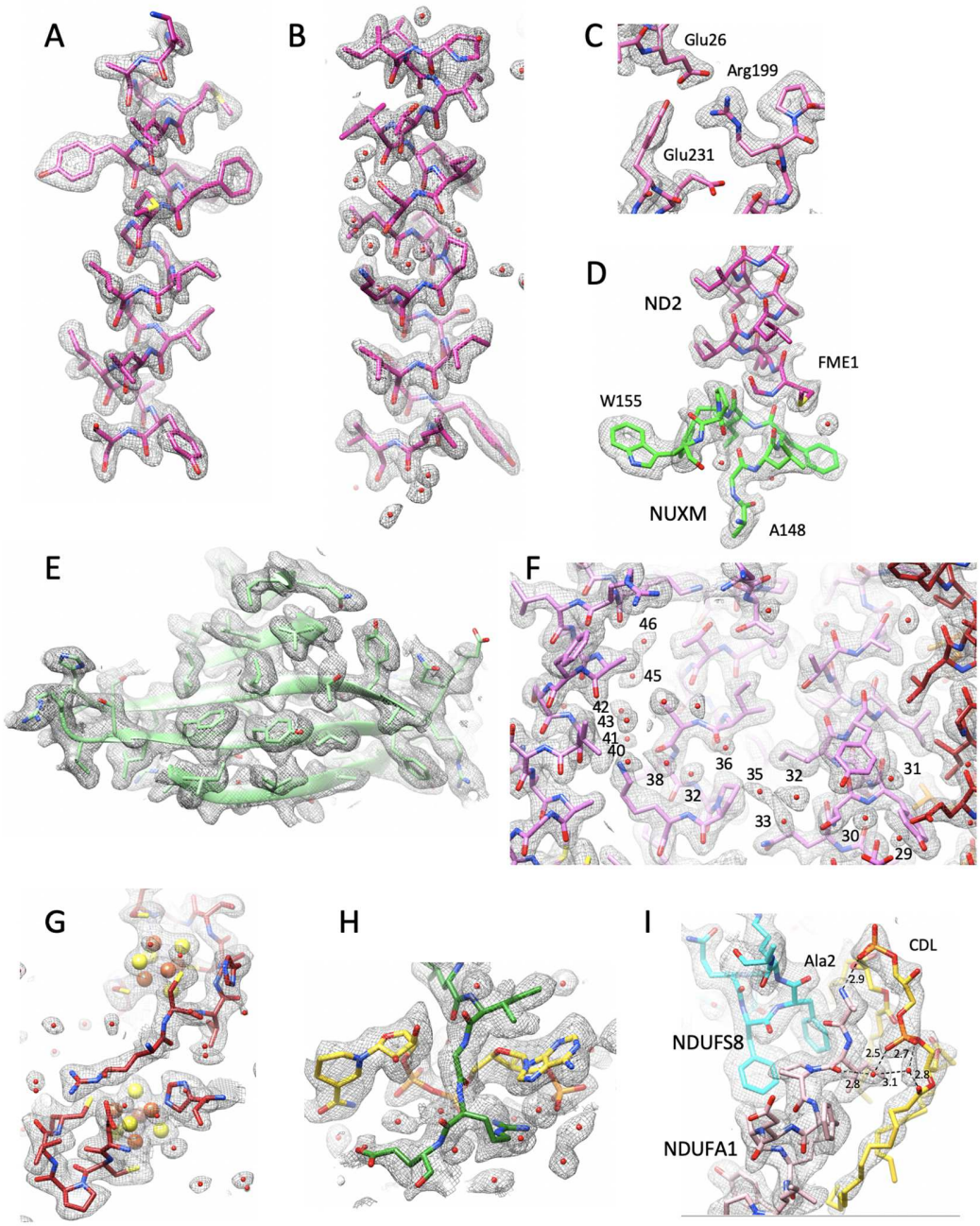

Fig. S2.

Examples of cryo-EM density of complex I at 2.1 Å resolution. **(A)** TMH ND2 152-171. **(B)** TMH ND2 229-249 with π-bulge. **(C)** salt bridge in ND1 with complete density for Glu26. **(D)** N-terminus of ND2 with formylmethionine, interacting with NUXM. **(E)** β sheet in NDUFS3. **(F)** Water molecules in the hydrophilic axis, labelled as in Figure S3. **(G)** FeS clusters in NDUFS1. **(H)** NADPH in NDUFA9. **(I)** Cardiolipin, coordinated by N-terminal Ala of NDUFA1; distances in Å are indicated.

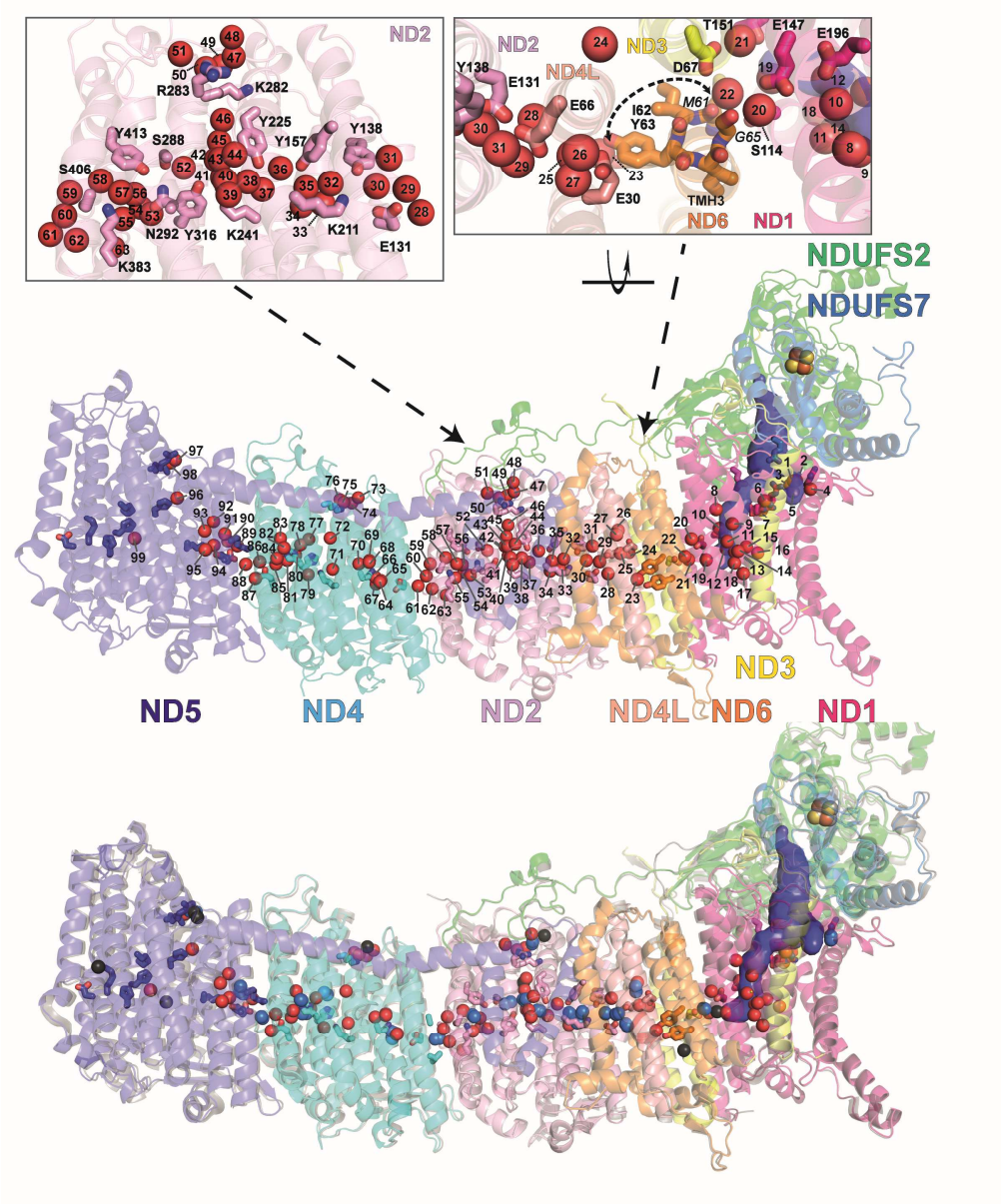

Fig. S3.

Water molecules in the membrane arm of *Y. lipolytica* complex I. Side view of central membrane bound subunits and central subunits NDUFS2 and NDUFS7 of the Q module as shown in Figure 2 with numbering scheme for the 99 water molecules (red spheres) resolved in the transmembrane region and at the entrance of putative proton uptake pathways. The upper left and upper right panel show detailed views of ND2 and centered around TMH3 of ND6, respectively. In the lower panel an overlay with the 2.7 Å structure of *(15)* (PDB ID: 6yj4; cartoon, gray) with water molecules in central membrane arm subunits (waters exclusively found in 6yj4, black spheres; waters exclusively found in this work, red; overlapping positions, blue) is shown.

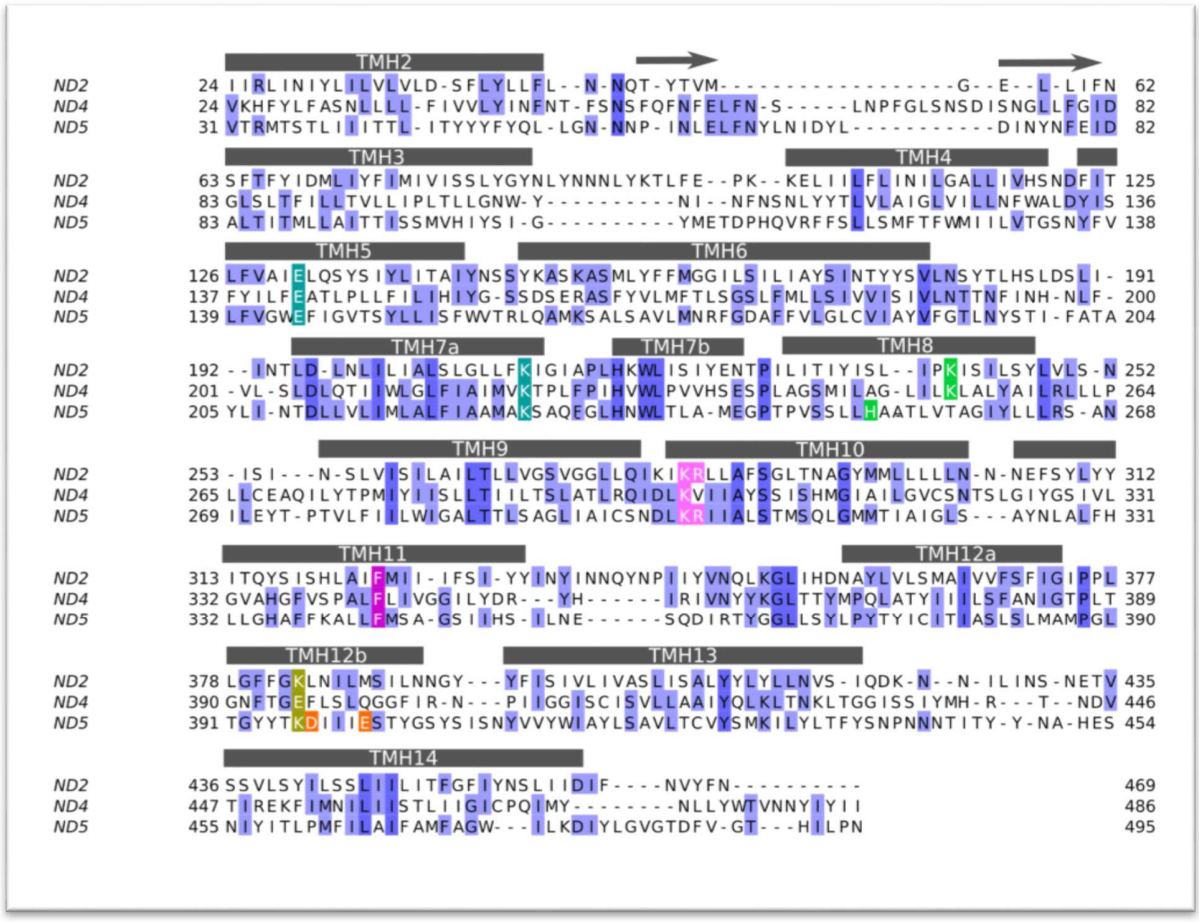

Fig. S4.

Multiple sequence alignment of antiporter-like subunits ND2, ND4 and ND5 from *Y. lipolytica*. The TM helices and the β-strands are indicated. The residues highlighted in shades of blue are colored by sequence identity. Amino acid residues discussed in the text are colored; conserved ion-pair from TMH5 and TMH7a (turquoise), conserved Lys/His residues from central hydrophilic axis (green), Lys/Glu from TMH12b (olive green), Asp and Glu from TMH12b (orange) that form proton releasing route in ND5, conserved residues of KR motif, a potential proton uptake site (pink) and conserved Phe from TMH11, a potential "gating" residue (magenta). The TMH1, TMH15 and the lateral helix of ND5 have been removed. Residue Lys511 from TMH15 of ND5 (not shown) is conserved in mitochondrial sequences, and participates in P-side connection of ND5 subunit. Alignment is based on the structural alignment of three subunits, and was prepared using Jalview *(59)*.

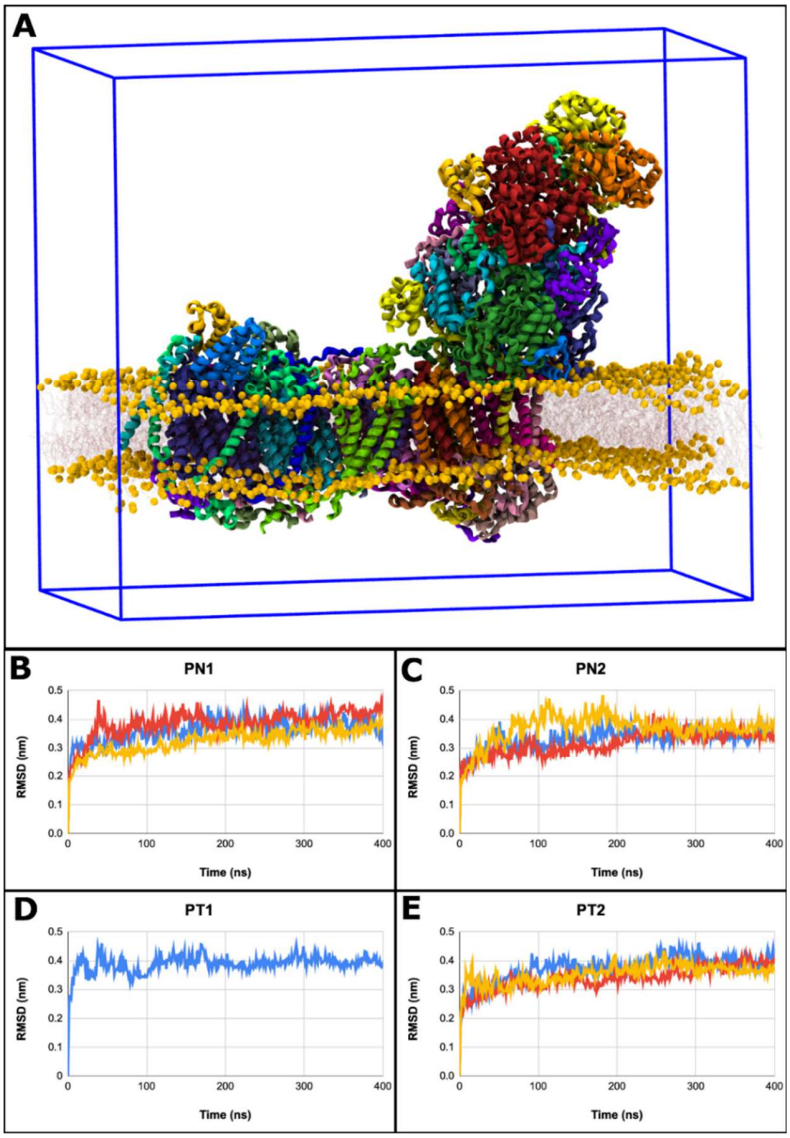

Fig. S5.

Molecular dynamics simulation setup and its stability. (A) Model system of respiratory complex I in membrane-solvent environment. Protein subunits are colored as in main text Figure 1. Lipid head groups are shown as orange spheres and lipid tails are shown in transparent red. The blue box shows the periodic boundaries, which is filled with water and Na and Cl ions (omitted for clarity). (B-E) Root mean square deviation (RMSD, in nm) was measured for the protein backbone atoms of all subunits for different simulation setups. The starting configuration (frame 0) of the simulation was used to align the trajectories, and as the reference for the calculation.

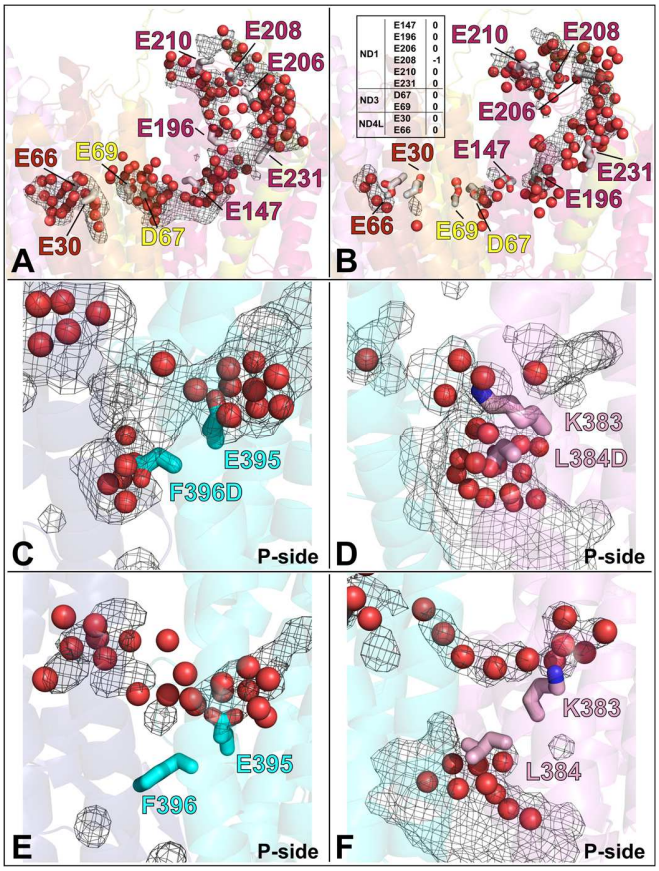

Fig. S6.

Hydration changes in the "E channel" region upon change in protonation states and induced opening of P-side connections in ND2/4 subunits. (A) For the E channel region (ND1, hot pink; ND3, yellow; ND4L, red; ND6, orange), the volumetric mesh is shown (in grey) from MD setup PN1 with all titratable residues in their charged states and (B) from MD setup PN2 with protonation states as in the inset table. Water molecules (red spheres) within 6 Å from residues shown in stick representation were selected from entire simulation data. The isovalue of the grey mesh in panels (A) and (B) is 0.20, and is calculated from all simulation replicas. (C) Effect of introducing F396D (ND4) and (D) L384D (ND2) *in-silico* point mutations on the hydration of the P-side regions of antiporter-like subunits. (E) Hydrophobic residues Phe396^{ND4} and (F) Leu384^{ND2} insulate the protein interior from the aqueous phase at the P side of the membrane in the wild-type enzyme. Panels (C) and (D) are from simulation setup PN3, while (E) and (F) are from PN1. Water molecules are shown within 6 Å of the mutated residues and selected residues shown in Figure 3A. The grey mesh was calculated by selecting water molecules within 6 Å from these selected residues from the entire simulation data (including all simulation replicas). The isovalue of the mesh is 0.10 in panels C-F. Water molecules are shown in red spheres and residues in sticks using pink (ND2) and cyan (ND4) for carbon atoms, blue for nitrogen and red for oxygen. Subunit coloring follows the same scheme as Figure 3A.

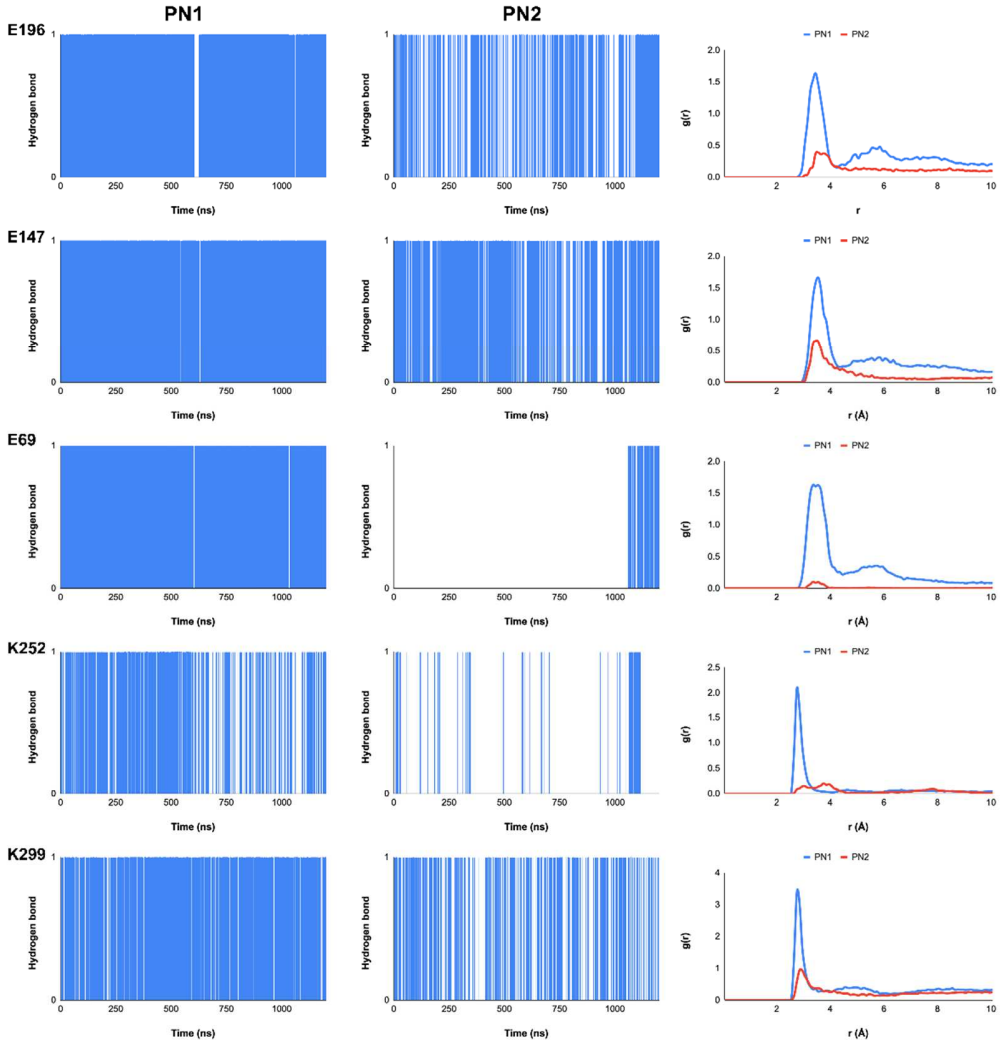

Fig. S7.

Water structure around a titratable residue in its neutral and charged states. Hydrogen bond between amino acid residue and water molecules and corresponding radial distribution function g(r), are shown for PN1 and PN2 simulations. In all cases, charged state of the residue stabilizes hydrogen bonds with water molecules compared to its neutral state. Data from selected residues are shown; E196 (ND1), E147 (ND1), E69 (ND3), K252 (ND4) and K299 (ND4). In hydrogen bond plots (data from three concatenated trajectories of 400 ns each, see Table S2), a value of y=1 or 0 corresponds to the presence or absence of a hydrogen bond calculated based on criteria (donor (D)-acceptor (A) distance 3 Å and D-H…A angle ≥160˚). The radial distribution function (PN1 – blue, PN2 – red) is calculated based on the distance (in Å) between nitrogen/oxygen atoms of sidechain of selected amino acid residue and oxygen atom of water molecules using data from all three simulation replicas.

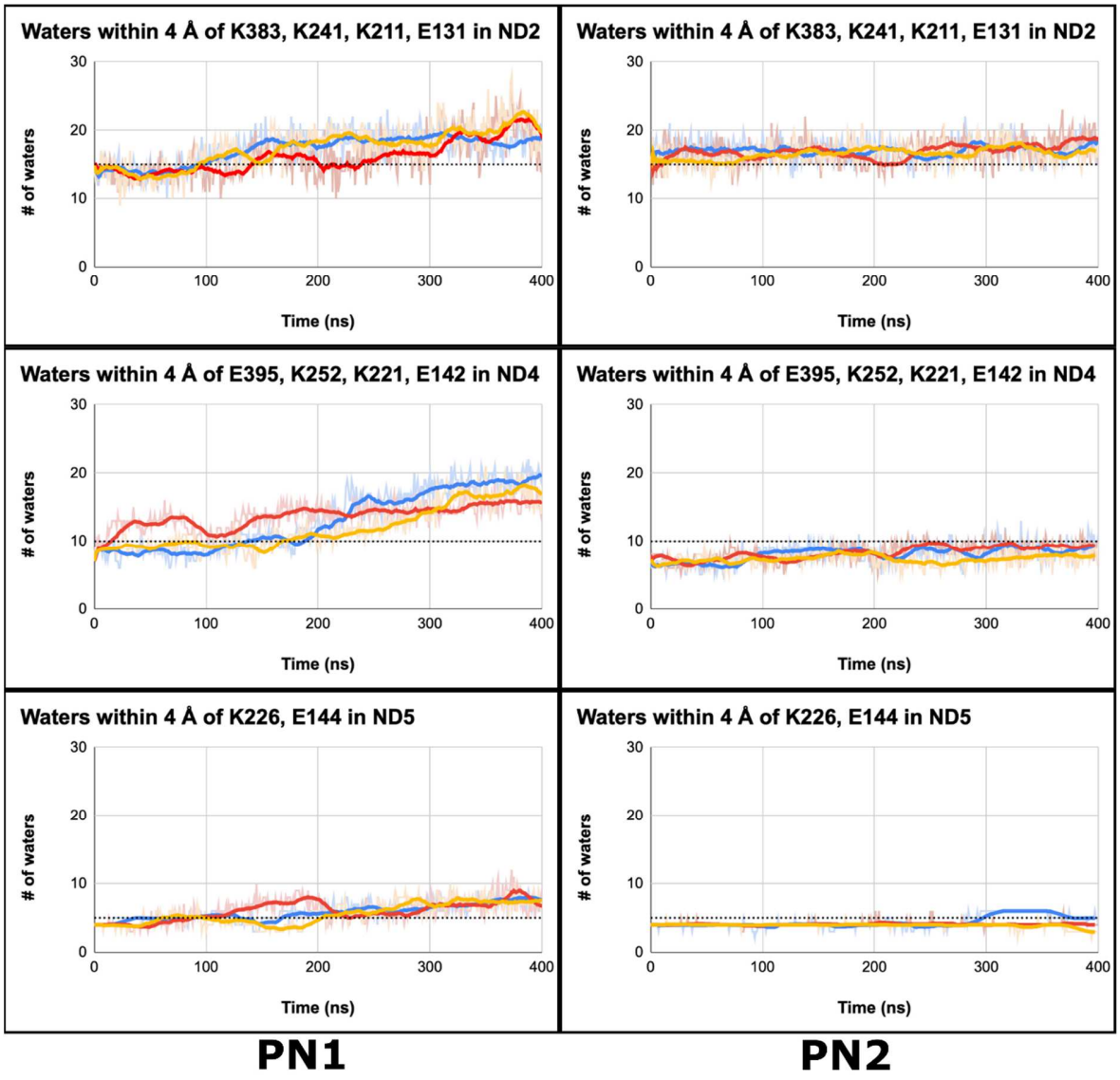

Fig. S8.

Convergence of water content in central hydrophilic axis of antiporter-like subunits. The left and right panels show number of water molecules from selected residues in central hydrophilic axis from PN1 and PN2 simulations, respectively. Data from PN2 simulations is closer to structural water content (shown by dotted lines). The three MD replicas are shown for each simulated state in different colors. The bold lines are running average over 20 simulation frames.

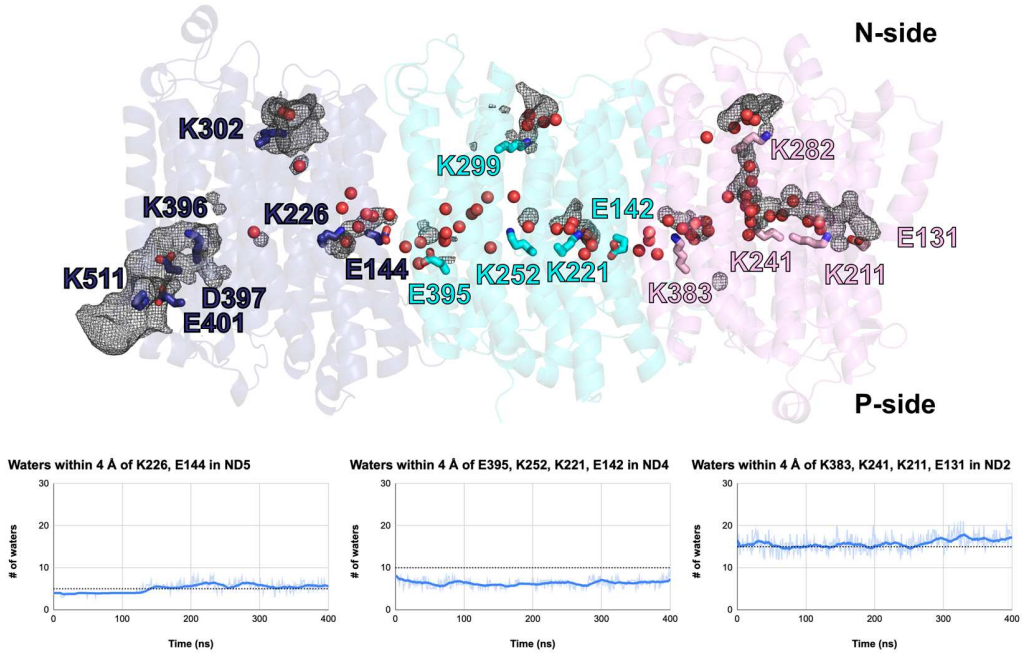

Fig. S9.
Hydration in antiporter-like subunits in MD simulations with AMBER force field. (Upper) Water molecules resolved in the cryo-EM map (red spheres) and hydrated regions observed in AMBER force field-based MD simulations (grey mesh) in subunits ND5 (dark blue), ND4 (cyan) and ND2 (pink). The volumetric map (grey mesh) is displayed at an isovalue of 0.15, from PN2 setup (Amber force field, see Table S2) by selecting water molecules within 6 Å from the labelled residues. (Lower) Convergence of water content in antiporter-like subunits. Plots show the number of water molecules from selected residues in central hydrophilic axis from PN2 (Amber force field, see Table S2) simulations is closer to the structural water content (dotted lines). The bold dark blue lines are running average over 20 simulation frames.

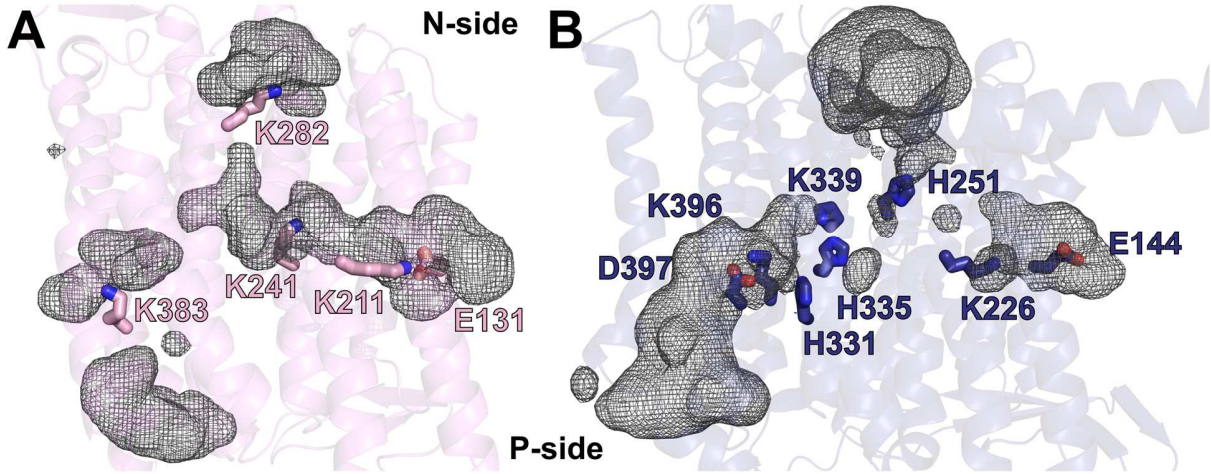

Figure S10.
Comparison of (putative) P side connections in antiporter-like subunits ND2 and ND5.
Average water occupancy map (grey mesh, isovalue 0.05) in subunits ND2 (A) and ND5 (B). A hydrated path from conserved K383 to the P side of the membrane does not form in ND2 subunit (A). In contrast, a strong hydration connects the homologous K396 to the P side of the membrane in ND5 subunit (B). A weak spherically-shaped water occupancy appears in ND2 subunit at very low isovalues (0.05), whereas water occupancy persists in ND5 subunit even at higher isovalues (see Fig. 3C). Water occupancy map is calculated from PN1 simulations (see Table S2) and data from all three replicas was combined. The occupancy map for ND2 was calculated by choosing water molecules within 6 Å from residues E131, K211, Y225, T233, K241, K282, S308, Y311, Y312, Y316, K383, N385 and Y413. For ND5, the occupancy map was calculated by choosing water molecules within 6 Å from the residues shown in Figure 3C.

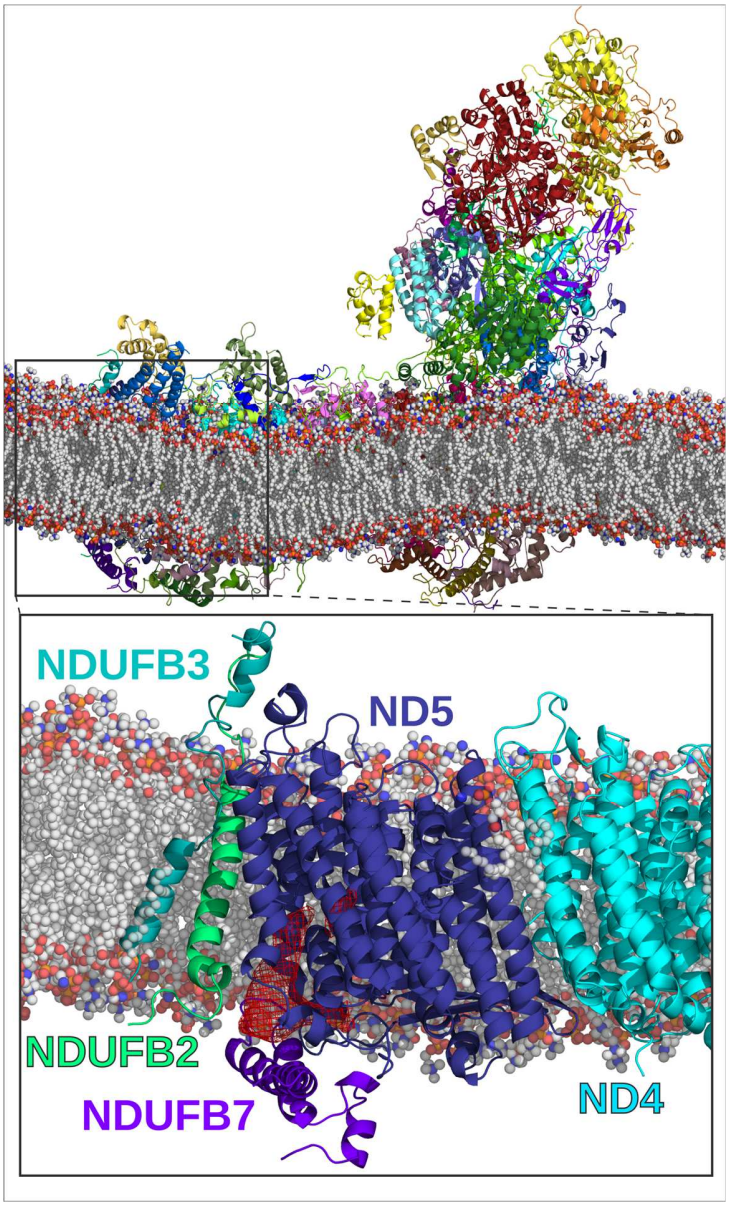

Fig. S11.
Membrane bending and lipid-protein interactions. Lipid bilayer bends and adjusts according to protein structure in MD simulations of complex I. **Inset** shows the unique lipid-protein architecture near putative proton exit route in ND5 subunit, in part induced by tilted TMHs of accessory subunits NDUFB3 and NDUFB2.

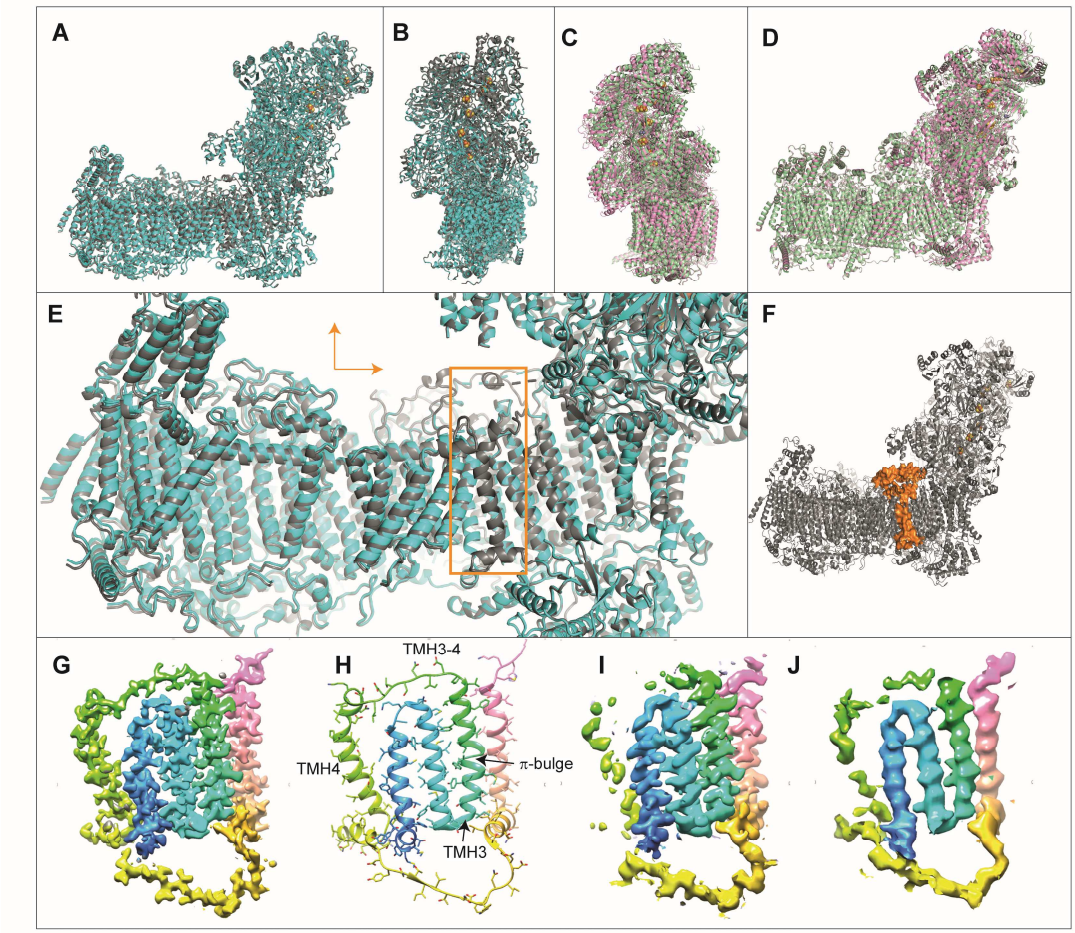

Fig. S12.

Overall conformational changes in complex I under turnover. (A) Sideview of *Y. lipolytica* complex I (deactive, gray; turnover, blue), **(B)** view from the backside, **(C,D)** same views as in (A,B) for an overlay of closed (pink, PDB ID: 6zkc) and open (green, PDB ID: 6zkd) state of ovine complex I (overlayed on subunit ND1), **(E)** same orientation as in (A) showing detailed view of the membrane arm, orange arrows indicate relative movement of P_D module, the orange box encloses an area with weak cryo-EM density for complex I under turnover, **(F)** orange surface highlights protein structure for which cryo-EM density is weak or missing for complex I under turnover, including a section of the long N-terminal extension of NDFUS2, the C-terminus of NDUFA9 and TMH4 and the TMH3-4 loop of ND6, **(G)** segmented map of ND6 from the 2.1 Å complex I map, **(H)** fitted model, **(I)** 3.4 Å map of ND6 under turnover (this work), **(J)** 4.5 Å map, EMD-4385 (Parey et al., 2018); G-J colored from blue (N-terminus) to pink (C-terminus). Under turnover, density for the TMH3-4 loop and for TMH4 is weak, indicating mobility of these regions, while TMH1-3 and TMH5 including the π-bulge region of TMH3 are rigid.

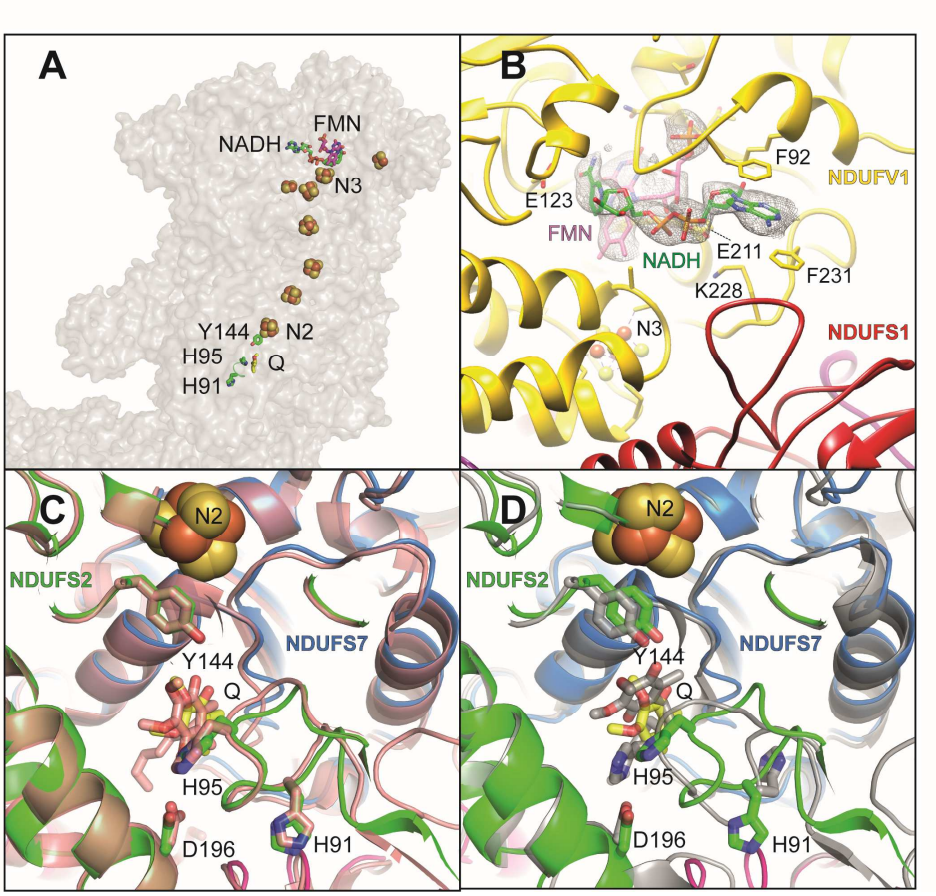

Fig. S13.

NADH oxidation and Q reduction site of complex I. (A) Topology of electron transfer reactions in the peripheral arm, **(B)** density for substrate NADH and the primary electron acceptor FMN in the NADH oxidation site, selected residues participating in NADH binding are shown in stick representation. **(C)** Q reduction site of *Y. lipolytica* complex I captured during steady state activity (DBQ, yellow; compare Figure 4) overlayed with complex I from sheep (salmon, PDB ID: 6zkc) and **(D)** with complex I from *T. thermophilus* (gray, PDB ID: 6i0d). In *Y. lipolytica* and ovine complex I the distance between the tyrosine residue near cluster N2 and Q is too long for a hydrogen bond. A different mode of Q binding is observed in complex I from *T. thermophilus* where Q is bound in a tyrosine – histidine ligation.

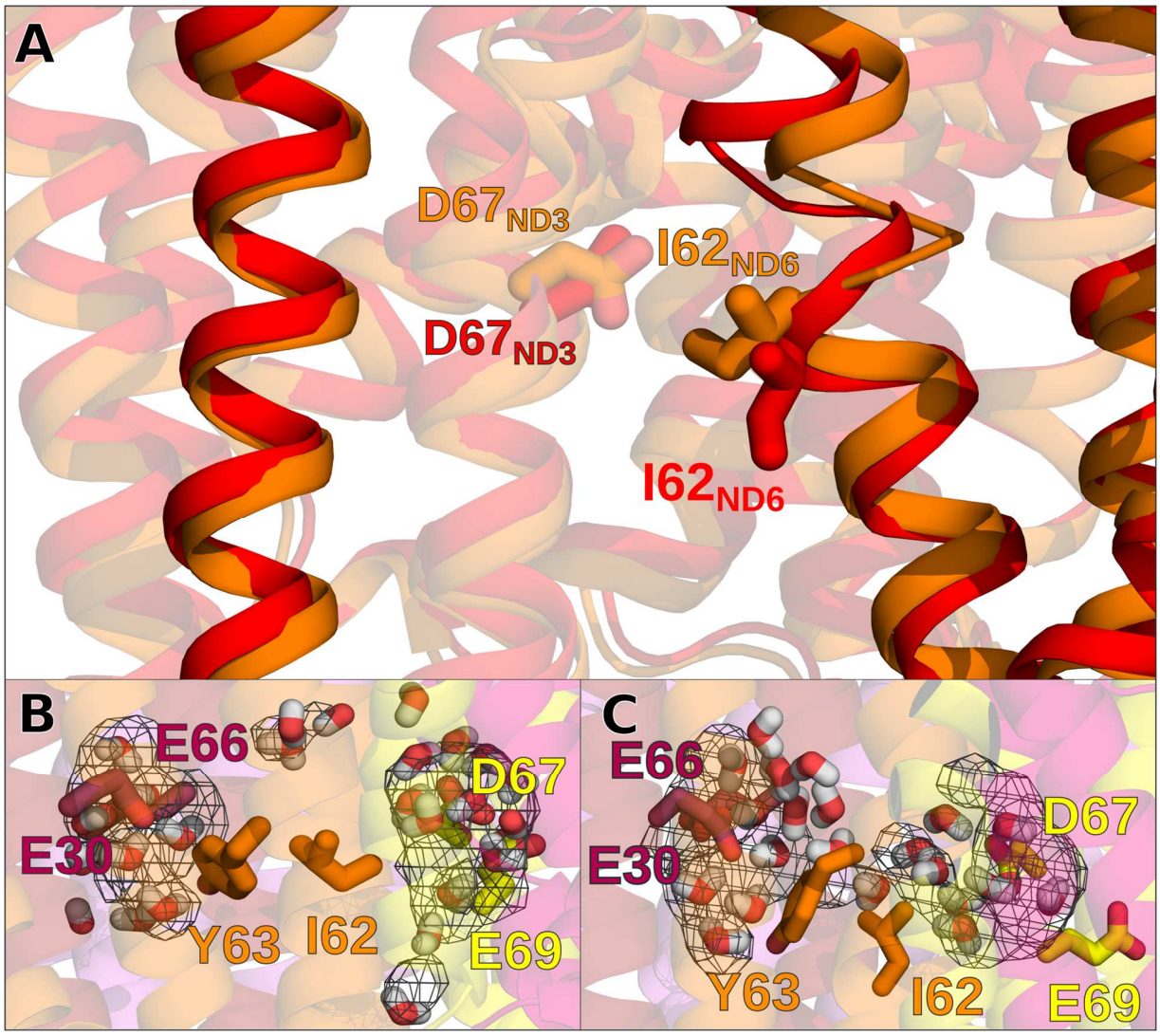

Fig. S14.

Hydration bridge between acidic residues of ND3 and ND4L. (A) Overlay of two MD simulation snapshots showing two conformations of Ile62 of ND6 subunit. Change in conformation of Ile62 and surroundings either closes **(B)** or opens **(C)** the route leading to water-influx in the dry region connecting conserved acidic residues of ND3 and ND4L subunits. The grey volumetric mesh (0.2 isovalue) representing water occupancy is calculated over entire simulation trajectory (setup PN1, simulation replica 3 for panel B and simulation replica 2 for panel C).

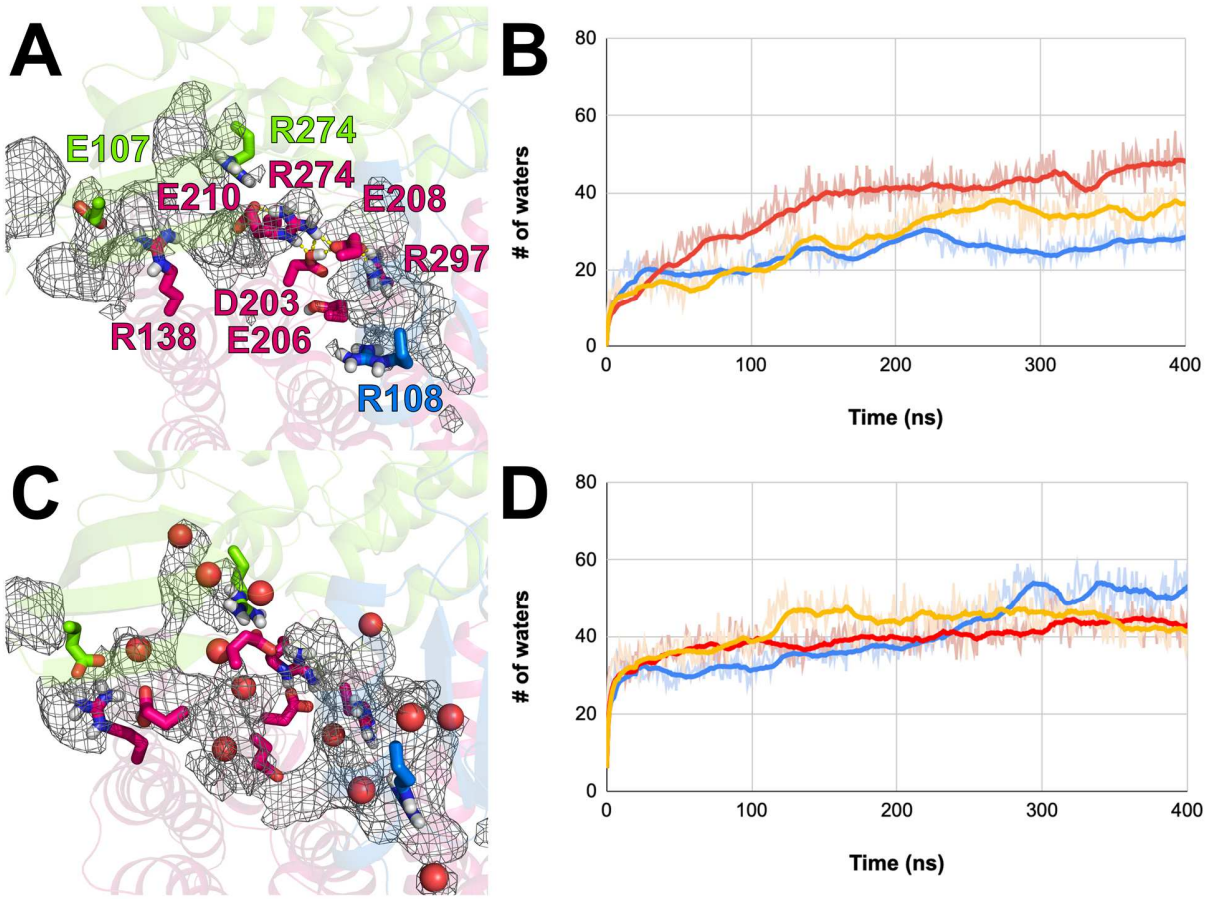

Fig. S15.
Water occupancy map and convergence of hydration at the interface of ND1 and Q module. The grey colored water occupancy map (A and C) and plots of water content (B and D) in the proposed novel "pumped" proton transfer route calculated from PT2 (top, A and B) and PN2 (bottom, C and D) simulations. The water occupancy map (grey mesh) is calculated by selecting water molecules within 6 Å of residues shown. Water content (water molecules within 6 Å of R138, D203, E208, E210, E206, R297 and R302 in ND1) with respect to simulation time is shown from three independent simulation replicas. Water content in the region stabilizes in all simulations, and converges well in PN2 simulations (based on higher resolution structure). The structural waters (red spheres) in the region are also displayed in panel C.

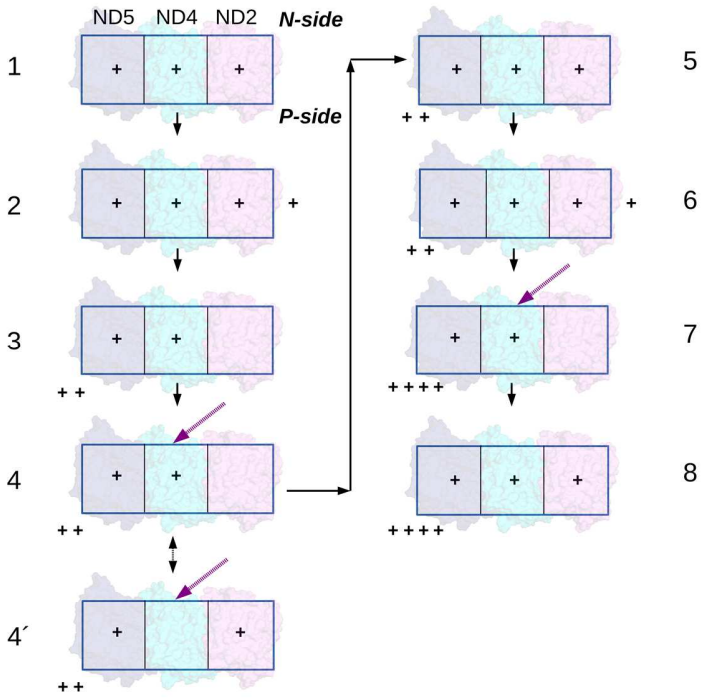

Fig. S16
Proposed mechanism of proton injection-driven proton pumping.
The three antiporter-like subunits are in their ground state (state 1) and are fully loaded with protons taken up from the N phase of the membrane. For simplicity, we say n = 3 protons (shown as "+") are loaded in the three antiporter-like subunits ND2/4/5. Protons may equilibrate/diffuse on the long hydrated central axis. Next, the proton from the proton loading site (PLS) arrives ("+" on the right, outside the boxes) in state 2, as a result of Q redox/protonation reactions (see Fig. 6). At this stage, the N-side paths in the antiporter-like subunits are closed (e.g. Phe gate identified, Fig. 3). Because of the electrostatic push of this arriving proton ("driver proton"), two protons are pushed out to the P side (state 3). Note that the protons are pushed to the P side from the middle of the antiporter-like subunits (half of the total membrane dielectric depth). In state 4, due to the release of the protons, the antiporter-like subunits are proton deficient, and as a result pick up a proton from the N side via paths that may open in response to this proton deficiency (purple dotted arrow). Since, antiporter-like subunits are connected via the central hydrophilic axis, proton uptake may occur via one of the antiporter-like subunits (state 4'). At this stage 4, a gating mechanism in ND5 subunit must be in place to prevent proton leak back from the P side to proton-deficient antiporter-like subunits (see also *(37)*). In state 5, the maximal proton loading capacity of antiporter-like subunits is reached again. In the next pump cycle, another driver proton from PLS drives pumping of two more protons, followed by uptake of a proton from the N side (state 7). The ground state is reached in state 8, ready for the next pump cycle. In this mechanism, four protons are pumped in one cycle, two are taken from the N side via antiporter-like subunits and two arrive as a result of Q redox/protonation chemistry, but taken from the N phase (Fig. 6). The horizontal protonic movements on titratable residues drive proton transfer across the membrane (see also *(4)*).

Table S1.
Data collection, refinement and model statistics.

	D form	**turnover**
Data collection		
Microscope	FEI Titan Krios	FEI Titan Krios
Camera	Gatan K3 Summit	Gatan K2 Summit
Voltage (kV)	300	300
Nominal magnification	165,000x	105,000x
Calibrated pixel size (Å)	0.516	0.828
Electron exposure ($e^-/Å^2$)	50.0	40.0
Exposure time total (s)	3	8
Number of frames per image	50	40
Defocus range (μm)	-0.8 – -2.2	-0.8 – -3.2
Image processing		
Motion correction software	*MotionCor2*	*MotionCor2*
CTF estimation software	*Gctf*	*Gctf*
Particle selection software	*RELION3.1*	*RELION3.0*
Micrographs (no.)	21,770	4,776
Initial particle images (no.)	1,078,966	124,092
Final particle images (no.)	178,960	54,863
Applied *B*-factor ($Å^2$)	-47	-62
Final resolution Relion (Å)	2.42	3.41
Final resolution denmod (Å)	2.12	-
Refinement statistics		
Initial model	6rfr	6rfr
Modeling software	*COOT, PHENIX*	*COOT, PHENIX*
Protein residues	8035	7921
Ligands	55	56
Waters	1617	-
Map CC (volume)	0.8181	0.8158
RMS deviations	0.005	0.007
Bond lengths (Å)		
Bond angles (°)	0.797	0.878
Ramachandran plot		
Outliers (%)	0.05	0.09
Favored (%)	96.88	96.46
Rotamer outliers (%)	2.88	0.56
Molprobity score	2.06	1.91
All-atom clashscore	9.81	14.92
PDB ID	**7o71**	**7o6y**

Table S2.
MD simulation setups.

	Structure for simulation setup	Charge state	Simulation time x no. of replicas
PN1	2.1 Å	Standard	400 ns x 3
PN2	2.1 Å	Propka-based	400 ns x 3
PN3	2.1 Å L384D (ND2) F396D (ND4) D397A (ND5)	Standard	400 ns x 1
PN4	2.1 Å TMH11 harboring F343 of ND4 modelled according to TMH11 harboring F324 of ND2	Propka-based[1]	400 ns x 1
PT1	3.4 Å	Standard	400 ns x 1
PT2	3.4 Å	Propka-based	400 ns x 3
PN1[2]	2.1 Å	Standard	400 ns x 1
PN2[2]	2.1 Å	Propka-based	400 ns x 1

[1]ND4 charges were set to replicate the ND2 charges calculated by Propka
[2]Simulations with AMBER force field (see methods).

Table S3.

Amino acid residues with non-standard protonation states (neutral charge state of Asp, Glu and Lys and positive charge state of His) based on Propka calculation.

Subunit	2.1 Å structure	3.4 Å structure
NDUFS1	D259	D146
	D295	D295
	D377	D377
	D556	D556
	E355	E355
	E420	E420
NDUFV1	D120	H378
	D420	D120
	E121	D420
	E142	E78
	E210	E121
	E291	E210
	K276	E291
		K276
NDUFS2	D196	D196
	D331	D331
	D363	D465
	D465	E107
	E151	E151
	E376	E165
	E379	E208
	E463	E218
		E379
		E404
		E463
NDUFS3	E179	E179
	K93	E181
		E227
		E237
		K93
NDUFV2	H28	H28
	E211	E211
	K68	
NDUFS8	E186	D163
		E137
		E186
		E195
ND1	E147	D203
	E196	E101
	E206	E147
	E210	E196
	E231	E206
	K285	E231
		K285
ND2	D39	D39
	D69	D69
	K282	K282

ND3	D67 E39 E69	D67 E39 E69
ND4	E142 E395 K252 K299	E58 E142 E237 E395 K252
ND5	D178 D397 E80 E503 K339 K581	D501 E80 E144 E271 E401 E453 K339 K581
ND6	K182	-
ND4L	D49 E30 E66	E30 E66
NDUFA9	H76 D210 E231	D210 E260
NDUFA5	H108 E92 E109 E110	E92 E110
NDUFS4	E72 K111	K111
NDUFA12	H78 D39	H78 D39
NDUFA6	-	E82
NDUFA2	K41	H62 E46
NDUFA11	-	H160
NDUFA13	H114 D7 E77	D7 E77
NDUFS5	E53	E18 E53
NDUFA1	H29	H29 E51 E83
NDUFB11	-	E189
NDUFB8	D74 E33	D59 D74 E33
NDUFB7	E58	H49 E55 E58
NDUFAB1	-	E94 E100
NDUFB10	E39	-

Movie S1.
Cryo-EM density (grey mesh) and model (protein in stick representation; inorganic sulfur, iron and water shown as spheres) close to FeS cluster N2 (same color scheme as in Figure 1).

Movie S2.
Global conformational changes in respiratory complex I of *Y. lipolytica*. The morph shows the change between complex I in the D form and complex I under turnover conditions. The P_D module slightly moves towards the matrix side and towards the P_P module. There are significant conformational changes at the junction of peripheral arm and membrane arm, most notably in ND1.

Movie S3.
Conformational changes in ND1 and in the Q binding site. The movie starts with a still image that shows labeling of selected residues. The morph between complex I in the D form and complex I under turnover conditions shows bending of TMH4 of ND1, conformational changes of the ND1 TMH5-6 loop and connected changes in and around the Q binding site. The following short sequence displays the position of the Q molecule in the turnover structure. The movie continues with restoration of the initial state.